Inorganic Chemistry

Article

pubs.acs.org/IC

Reversibly Tunable Upconversion Luminescence by Host–Guest Chemistry

Takaaki Taniguchi,*[,†,‡] Tomoaki Murakami,[†] Asami Funatsu,[†,‡] Kazuto Hatakeyama,[†,‡] Michio Koinuma,[†,‡] and Yasumichi Matsumoto[†,‡]

[†]Graduate School of Science and Technology, Kumamoto University, 2-39-1 Kurokami, Kumamoto 860-8555, Japan

[‡]CREST, Japan Science and Technology Agency (JST), 7 Gobancho, Chiyoda-ku, Tokyo 102-0075, Japan

Supporting Information

ABSTRACT: Tuning upconversion (UPC) luminescence using external stimuli and fields, as well as chemical reactions, is expected to lead to novel and efficient optical sensors. Herein, highly tunable UPC luminescence was achieved through a host–guest chemistry approach. Specifically, interlayer ion exchange reactions reversibly tuned the emission intensity and green-red color of Er/Yb-codoped $A_2La_2Ti_3O_{10}$ layered perovskite, where A corresponds to proton and alkali metal ions, enabling the visualization of host–guest interactions and reactions.

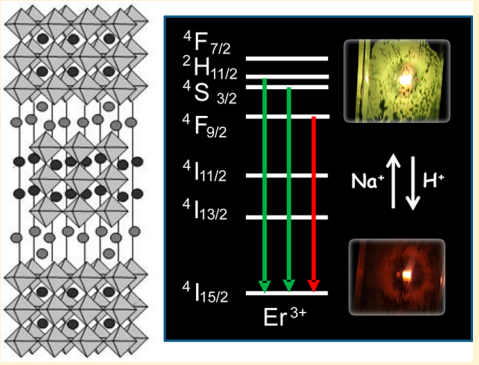

INTRODUCTION

Materials containing Er^{3+} or Tm^{3+} dopants can produce blue, green, and red upconversion (UPC) luminescence via near-infrared excitation.[1] Over the past decade, many studies have focused on the size, shape, and phase-controlled synthesis of Er(Tm) and Yb codoped UPC nanoparticles for potential bioimaging applications.[2−5] More recently, the development of optical sensor based UPC materials, in which the total emission intensity and color are reversibly modulated by external fields or environment, has received much attention.[6−8] For example, the UPC luminescent intensity of $NaGdF_4$–Er/Yb/Nd depends on the magnetization of the paramagnetic Gd^{3+} ions,[9] making these phosphors potential magnetic field sensors. In addition, Gd_2O_3–Er/Yb and Yb_2TiO_7–Er/Mo can be used as luminescent thermometers because the excited energy levels $^2H_{11/2}$ and $^4S_{3/2}$ of Er^{3+} present a quasi-thermal equilibrium.[10,11] Hao et al. have reported that the electrical control of the Er^{3+} site symmetry in the ferroelectric $BaTiO_3$ matrices reversibly changed the radiative transition probabilities and, therefore, changed the UPC luminescence of epitaxial $BaTiO_3$–Er/Yb films.[12] Besides, Sun et al. have utilized resonant surface plasmon polariton waves to modulate UPC luminescence of $NaYF_4$–Er/Yb.[13] However, no study has exploited chemical reactions to reversibly tune UPC luminescence by direct modification of electron–phonon coupling.

Nanostructured crystals that involve a periodic nanospace in their crystalline framework, such as metal–organic frameworks (MOFs),[14,15] zeolites,[16,17] and layered compounds,[18] are expected to provide an interesting playground for chemically tuning UPC properties. These nanostructured crystals can store and release ions, molecules, and clusters by host–guest reactions, which provides a wealth of opportunities for engineering new functional materials with tunable properties. The combination of host–guest reactions and UPC luminescence may lead to tunable photoluminescent (PL) systems that may find applications in highly sensitive and selective sensors with low scattering and low damage on biosystems.

Herein, we demonstrate for the first time the UPC luminescence reversibly and ratiometrically tuned via host–guest reactions. The layered perovskite with a Ruddlesden–Popper phase $K_2La_2Ti_3O_{10}$ (K-LTO), which consisted of three double-octahedral $La_2Ti_3O_{10}$ (LTO) perovskite layers and K^+ interlayer ions,[19] was selected as a host material (Figure 1a). This choice was directed by (1) the facile Er^{3+}/Yb^{3+} doping at La^{3+} sites, (2) extremely thin thickness of perovskite layers potentially maximizing host–guest optical coupling, and (3) ready substitution of interlayer K^+ ions with protons (H^+) and alkali metal ions. The recognition abilities of these elements can be harnessed for biochemical and radiological sensing.

EXPERIMENTS

Sample Preparation. *Er^{3+}/Yb^{3+} Codoped $K_2La_2Ti_3O_{10}$ (K-LNO).* Stoichiometric amounts of La_2O_3, TiO_2, Er_2O_3, and Yb_2O_3, and 20 mol % excess K_2CO_3 were mixed and then annealed at 900 °C for 4 h in air. Then, the products were crushed and mixed again. Finally, the mixtures were annealed at 1100 °C for 11 h in air.

Er^{3+}/Yb^{3+} Codoped $KLaNb_2O_7$ (K-LNO). Stoichiometric amounts of La_2O_3, Nb_2O_5, Er_2O_3, and Yb_2O_3, and 20 mol % excess K_2CO_3 were

Received: May 22, 2014
Published: August 14, 2014

   dx.doi.org/10.1021/ic501129y | Inorg. Chem. 2014, 53, 9151−9155

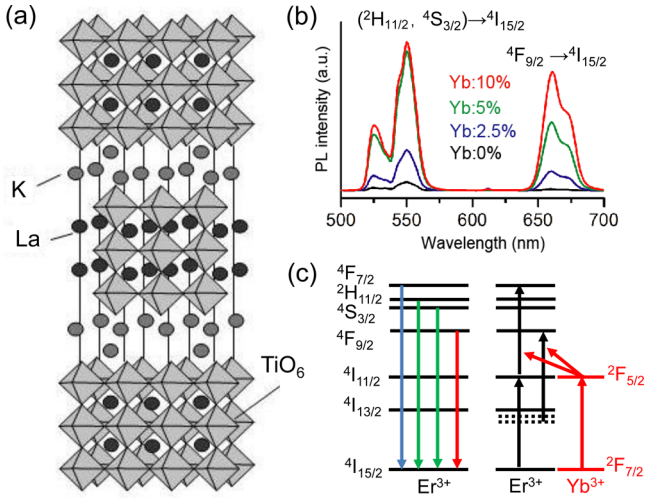

Figure 1. (a) Scheme of the K-LTO structure. (b) Visible UPC luminescence spectra of K-LTO codoped with 2.5 mol % Er^{3+} and 0, 2.5, 5, and 10 mol % Yb^{3+} (excitation wavelength, 980 nm; excitation laser output power, 1 W/cm^2). (c) Representative energy transfer mechanism in upconversion luminescence in an Er^{3+}/Yb^{3+} system.

mixed and then annealed at 900 °C for 4 h in air. Then, the products were crushed and mixed again. Finally, the mixtures were annealed at 1100 °C for 40 h in air.

The 2.5 mol Er^{3+}/10 mol Yb^{3+} Codoped YF_3. A total of 3.5 mmol of YCl_3 (Wako, 99.5%) and $YbCl\cdot 8H_2O$ and $ErCl_3\cdot 8H_2O$ (Wako, 99.5%) was dissolved in distilled water (15 mL) at room temperature. Subsequently, 10 mL of aqueous NH_4F solution (12 mmol, Aldrich, 99.98%) was added. The precipitates were collected and then dried at 80 °C in air. Finally, the products were annealed at 400 °C for 5 h in air.

Proton Exchange. $K_2La_{1.95-2x}Er_{0.05}Yb_{2x}Ti_3O_{10}$ (K-LTO) was reacted with 0.1 M HCl for 1 week with vigorous sintering. K-LNO was reacted with 1 M HCl for 4 weeks with vigorous sintering. In all cases, the acid was replaced daily to ensure complete exchange.

Characterization. The crystalline products obtained were characterized by powder X-ray diffraction (XRD) using a Rigaku Miniflex II powder diffraction system with Cu Kα radiation (λ = 0.154178 nm). Scanning electron microscopy (SEM) with EDX analyzer was performed on an FEI XL30 Sirion scanning electron microscope. PL spectra were obtained using a spectrofluorometer (Jasco FP-6500). The luminescence spectra of the sample were measured under excitation by a 980 nm continuous wave (CW) laser diode (LD) (L9418-04, Hamamatsu Photonics) equipped with a temperature controller (TED200, Thorlabs). Visible−near-infrared absorption spectra of the samples were measured with a spectrometer (UV-3600 Shimazu). For each measurement, a $BaSO_4$ plate was uniformly covered with 0.4 g of sample powder, and then the reflection spectra was measured.

RESULTS AND DISCUSSION

The synthesis of $K_2La_{1.95-2x}Er_{0.05}Yb_{2x}Ti_3O_{10}$ (x = 0, 0.025, 0.05, or 0.1) was carried out using a conventional solid-state procedure The synthesized materials presented XRD patterns that corresponded well to the $K_2La_2Ti_3O_{10}$ and $K_2La_2Ti_3O_{10}\cdot H_2O$ phases (Figure S1, Supporting Information),[19] indicating that, regardless of their concentrations, the rare earth ions (Er^{3+} and Yb^{3+}) substituted well for La^{3+} ions because of their similar ionic radii. Note that K-LTO is hygroscopic, forming hydrates, $K_2La_2Ti_3O_{10}\cdot H_2O$ phases, on exposure to air. SEM analysis showed that micron-sized plate-like products were formed (Figure S2, Supporting Information).

Figure 1b shows the UPC luminescence spectra of a series of K-LTO−Er/Yb samples excited at 980 nm with a continuous laser diode (1 W/cm^2). The PL peaks at 500−575 and 630−700 nm regions were assigned to the ($^2H_{11/2}$, $^4S_{3/2}$) → $^4I_{15/2}$ and $^4F_{9/2}$ → $^4I_{15/2}$ transitions, respectively (Figure 1c).[1] This detected visible luminescence is well explained by UPC mechanisms based on energy transfer upconversion and excited-state absorption. Yb^{3+}-codoping significantly enhanced the UPC luminescence, which was clearly visible to the naked eye. The sensitization effect results from the quasi-resonance between the $^2F_{5/2}$ energy level of Yb^{3+} and the $^4I_{11/2}$ energy level of Er^{3+}. At 980 nm, Yb^{3+} exhibited a considerably higher absorption cross-section than for Er^{3+}, allowing the pump energy to be efficiently absorbed and transferred to Er^{3+}. The increase in Yb^{3+} concentration generally enhanced the red light emission ($^4F_{9/2}$ → $^4I_{15/2}$ radiative transition) because of the ($^2H_{11/2}$ + $^4I_{13/2}$) → ($^4F_{9/2}$ + $^4I_{15/2}$) cross-relaxation process between Er^{3+} ions.[1] Er/Yb codoped $KLaNb_2O_7$ (K-LNO) with a single-layered perovskite structure yielded a predominant green emission band due to ($^2H_{11/2}$, $^4S_{3/2}$) → $^4I_{15/2}$ transitions without any remarkable Yb^{3+} codoping effects resulting in the negligible activation of the Er^{3+}−Er^{3+} energy transfer in the single perovskite $LaNb_2O_7$ (LNO) unit in K-LNO (Figure S3, Supporting Information). By analogy, the two-dimensional anisotropy of LTO units is therefore not the main reason for the activation of Er−Er energy transfer by Yb codoping.

The intercalated K^+ ions were subsequently exchanged with protons by vigorous sintering in the presence of 0.1 M HCl for 1 week. Figure 2a shows UPC−PL spectra for LTO−Er/Yb

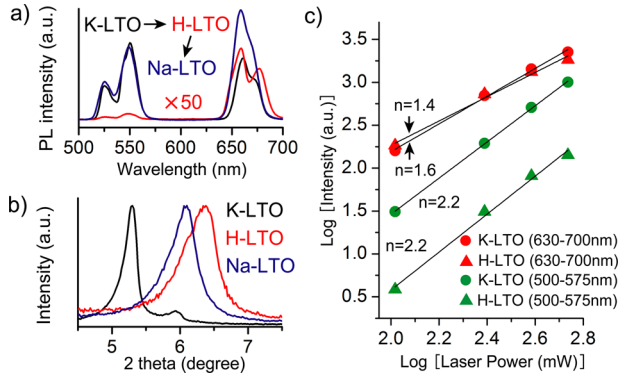

Figure 2. (a) Visible UPC luminescence spectra and (b) (001) or (002) XRD peaks of K-LTO, H-LTO, and Na-LTO codoped with 2.5 mol % Er^{3+}/10 mol % Yb^{3+}. (c) Plot (ln−ln) of emission intensity versus excitation power of K-LTO and H-LTO doped with 2.5 mol % Er^{3+}/10 mol % Yb^{3+}.

samples (Er, 2.5%; Y, 10%) before and after protonation. Remarkably, the emission intensity of K-LTO decreased by approximately 1/100 upon proton exchange. XRD analysis confirmed that a protonated LTO (H-LTO) phase was produced without any secondary phase formation, such as La- or Ti-based oxides and hydroxides (Figure S1, Supporting Information). In the H-LTO structure, the intercalated H^+ ions bind the terminal oxygen ions of the semicuboctahedral cavity to form OH bonds.[19] Because of the thickness of the double perovskite layer (1.1 nm), the electronic states of the Er^{3+} and Yb^{3+} ions in LTO units strongly couple with the high-energy OH vibration (3500 cm^{-1}), enhancing the nonradiative transition rate to a great extent.

dx.doi.org/10.1021/ic501129y | Inorg. Chem. 2014, 53, 9151−9155

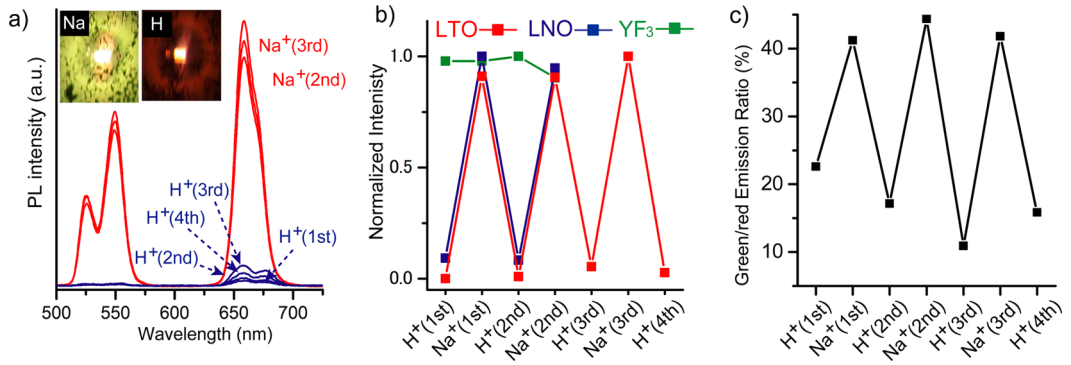

Figure 3. (a) Change in visible UPC luminescence spectra of 2.5 mol % Er^{3+}/10 mol % Yb^{3+} codoped LTO. (b) Integrated emission intensity of 2.5 mol % Er^{3+}/10 mol % Yb^{3+} codoped LTO, LNO, and YF_3 by a cyclic H^+−Na^+ exchange. (c) Green/red emission ratio of 2.5 mol % Er^{3+}/10 mol % Yb^{3+} codoped LTO by a cyclic H^+−Na^+ exchange.

The green-to-red light emission color change is another notable feature observed upon protonation. The red light emission ($^4F_{9/2} \rightarrow {}^4I_{15/2}$ transition) got visibly stronger than the green light emission ($^2H_{11/2}$, $^4S_{3/2} \rightarrow {}^4I_{15/2}$ transitions; Figure 2a). Figure 2c shows the plots of ln(emission intensity) versus ln(pump power) monitored at green (550 nm) and red (660 nm) light emissions. For a UPC process, the intensity of the UPC luminescence is proportional to some power n (2, 3, etc.) of the incident pump laser intensity, where n is the number of pump photons absorbed per photon emitted. Linear fits of provided slopes (n) of 2.2 and 1.6 for green and red light emissions of K-LTO, respectively. The H-LTO sample showed n values similar to K-LTO for each emission (2.2 and 1.4 for ($^2H_{11/2}$, $^4S_{3/2}$) and $^4F_{9/2} \rightarrow {}^4I_{15/2}$ transitions, respectively). Although the slope values less than 2.0 indicated that experimental errors were involved for these measurements, these results suggest that the relaxation processes that produced these emissions in LTO units were rather independent of the interlayer species. In contrast, the transition rates were greatly influenced by the interlayer vibrational state, enabling a ratiometric color change by K^+−H^+ exchange reaction. Upon proton exchange, the depletion of low-lying intermediate levels (for example, $^4I_{11/2}$ of Er^{3+}) by OH^- quenching suppresses the population in high-lying levels ($^4F_{7/2}$ of Er^{3+}) by subsequent excited state absorption or energy transfer. Therefore, the emission in the green region involving a high number of excitation steps should be more sensitive to OH^- quenching than the emission in the red region involving fewer excitation steps.

If the UPC−PL quenching originates from the high-energy vibration of interlayer OH groups, a subsequent metal exchange process should restore the PL efficiency of LTO−Er/Yb as a result of the decoupling of high-energy OH vibration and Er^{3+}/Yb^{3+} energy levels. A Na^+ ion exchange reaction was performed to validate this hypothesis. In this process, H-LTO was dispersed in 1 M NaOH solutions for 12 h with vigorous stirring. As expected, the Na^+ exchange drastically enhanced the PL intensity more than 100 fold (Figure 2a). Indeed, an enhancement of the intensity ratio between green and red emission bands was visible upon Na^+ ion-exchange. Accompanying the PL change, the low-angle XRD peak shifted toward higher and lower angles by HCl and the subsequent NaOH treatments (Figure 2b), indicating that interlayer distance decreased and then increased by HCl and the subsequent NaOH treatments. Indeed, the overall XRD pattern of the NaOH-treated sample (Figure S4, Supporting Information) corresponds to an anhydrous $Na_2La_2Ti_3O_{10}$ phase. SEM-EDX observation showed that the Na^+ ions were homogeneously involved in LTO plates with a Na/La ratio of 0.6 (Figure S5, Supporting Information), which further confirmed that the K^+/H^+/Na^+ ion exchange reactions resulted in the dramatically modulated PL properties.

The H^+−Na^+ exchange reaction was performed over several cycles, enabling the repeated modulation of emission intensity and green−red color ratio (Figure 3a). The same measurement conditions, including the excitation power, sample position, amount, slits width, and detection sensitivity, were employed for these experiments. We also confirmed that the absorption cross section at 980 nm was almost unchanged by H^+−Na^+ exchange (Figure S6, Supporting Information). The resulting on/off the UPC−PL intensity ratio amounted to approximately 75, which was more than 1 order larger compared to ratios obtained by magnetic (ca. 2),[9] electric (ca. 3),[12] and plasmonic (ca. 6)[13] tuning at room temperature. LNO−Er^{3+}/Yb^{3+} also exhibited a reversibly tunable UPC emission by a cyclic H^+−Na^+ exchange with the on/off ratio of ca. 10 (Figure 3b and Figure S7a, Supporting Information). However, a YF_3−Er^{3+}/Yb^{3+} sample did not present any PL change upon reaction with HCl and NaOH solutions (Figure 3b and Figure S7b, Supporting Information), indicating that a highly tunable UPC emission is hard to achieve through surface chemical reactions. It is remarkable that the large emission on/off ratio observed in H^+−Na^+ exchange reactions of the layered perovskites can offer an extreme example to understand the size or surface effects on UPC−PL properties of nanophosphors. For a decade, surface quenching has severely hampered the application of UPC nanoparticles. For example, the UPC efficiency of $NaGdF_4$−Yb/Tm nanoparticles (10 nm) increased as high as 60 times upon formation of a 2.5 nm thick $NaGdF_4$ shell owing to the removal of surface ligand and defects.[20] By considering two-dimensional LTO units as excised 1 nm thick crystal surfaces, our results suggest that the presence of surface OH^- ligands can reduce the luminescent efficiency at the outermost surface region of UPC nanoparticles 100 times, even without any contributions from structural defects.

Cation exchange reaction of H-LTO in the presence of Li^+ ions also led to the similar concurrent increase in total PL intensity and green-to-red emission ratio (Figure S8, Supporting Information). In contrast, reactions between H-LTO and other alkaline earth metal ions (K^+ and Cs^+) did not enhance the PL intensity (Figure S8, Supporting Information). We investigated the reason the reactions of H-LTO with K^+

dx.doi.org/10.1021/ic501129y | Inorg. Chem. 2014, 53, 9151−9155

and Cs^+ ions gave no PL enhancement. First, we hypothesized that narrow interlayer galley of H-LTO prevented the insertion of alkaline metal ions with larger ionic diameters than Na^+ into the interlayer nanospace. However, SEM-EDX observation revealed that the K^+ ions were homogeneously distributed in LTO plates with a K/Ti ratio of 0.7 (Figure S5, Supporting Information). Thus, H^+ ions in H-LTO were exchanged with K^+ ions. Importantly, XRD analysis revealed that the XRD pattern of the KOH-treated sample corresponds to hydrous $K_2La_2Ti_3O_{10}\cdot H_2O$ phases (Figure S4, Supporting Information),[19] and the XRD pattern of the CsOH-treated sample is almost identical with that of KOH-treated one. Therefore, H_2O molecules were additionally inserted in the LTO interlayer galley during K^+ or Cs^+ exchanging. As a result, OH vibration of interlayer H_2O molecules strongly coupled with the electronic states of the Er^{3+} and Yb^{3+} ions so that the UPC luminescence was not recovered by the exchange process. We confirmed that heat treatment of as-synthesized K-LTO−Er^{3+}/Yb^{3+} at 70 °C in humid condition (relative humidity (RH) of ca. 90%) resulted in strong UPC quenching due to the complete hydration of LTO (Figure S4, Supporting Information). These results demonstrate that UPC luminescence in layered perovskites is highly sensitive to interlayer molecules in addition to interlayer cations, which may extend the range of potential applications of tunable luminescence by host−guest chemistry approach.

Exchange reaction kinetics was investigated by monitoring the UPC−PL intensity during the reaction of H-LTO−Er/Yb with 1 M MOH solutions (M = Li, Na, K, and Cs). Figure 4a,b

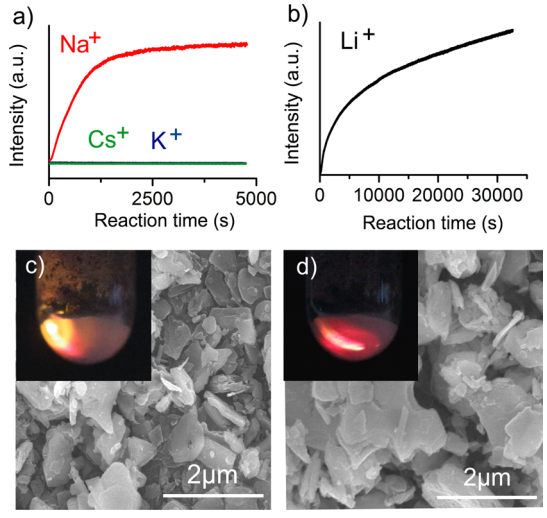

Figure 4. In situ kinetic analysis of (a) H^+−(Na^+, K^+, Cs^+) and (b) H^+−Li^+ exchange reactions by monitoring 540 nm UPC luminescence of 2.5 mol %Er^{3+}/10 mol %Yb^3 codoped H-LTO. UPC emission and SEM images of LTO−Er/Yb powders at the (c) upper and (d) bottom sides of the centrifuge tube after the reaction with 1 M Na(OH) solution for 10 min.

displays changes in PL intensity monitored at 540 nm as a function of reaction time. In general, the PL intensity increased with reaction time because of the progressive removal of interlayer OH bonding upon Li^+ and Na^+ exchange, while reaction with KOH and CsOH resulted in no PL enhancement. The emission intensity almost reached saturation after 2500 s during the Na^+ exchange reaction. On the other hand, the emission intensity kept on increasing even for reaction times exceeding 50 000 s for Li^+ exchange reactions. This is because Li^+ is more strongly hydrated in aqueous solutions than Na^+, which significantly lowers the Li^+ exchange rate. These data demonstrate that UPC−PL can be utilized for the high-sensitivity in situ analysis of host−guest reaction kinetics.

Finally, the ratiometric color change depending on the interlayer composition was employed to visualize the local reaction kinetics. When the Na^+ exchange process was performed with 1 M NaOH solution for 10 min and the resulting dispersion was centrifuged, the collected sediments showed an emission color that gradually changed from the bottom to the upper sides of the centrifuge tube (Figure 4c,d). This result suggests that small grains, located in the upper part, were readily Na^+ exchangeable and produced a yellowish emission while the larger ones located at the bottom exhibited slower kinetics for this reaction because of their longer diffusion length. Consequently, a red light emission resulting from a higher interlayer H^+ concentration was observed at the bottom of the tube. SEM observations confirmed that the average particle size of the product at the bottom was apparently larger than that at the top (ca. 1 μm) (Figure 4c,d), providing evidence that multicolor UPC emission is utilized for the ratiometric imaging of host−guest reaction kinetics and interactions.

CONCLUSION

The reversible tuning of UPC luminescence of Er^{3+}-activated layered perovskite materials through host−guest reactions was reported. LTO−Er/Yb exhibited a large on/off UPC−PL intensity ratio because of the strong host−guest vibrational coupling with green−red ratiometric emission change. The LTO−Er/Yb enabled the high-sensitivity in situ and local analysis of the ion exchange reaction kinetics. In addition to the layered metal oxide, MOF and zeolite frameworks exhibit one-, two-, and three-dimensional nanospaces that can be fine-tuned to store and release various kinds of ions and molecules. Activating the UPC properties of these materials by Er, Tm, and Yb doping will further offer an attractive means to visualize host−guest reactions and develop novel sensing and imaging materials.

ASSOCIATED CONTENT

Supporting Information

XRD patterns, SEM images, visible−near-infrared absorption spectra, visible UPC luminescence spectra, SEM-EDS images. This material is available free of charge via the Internet at http://pubs.acs.org.

AUTHOR INFORMATION

Corresponding Author

*E-mail: taktani@gpo.kumamoto-u.ac.jp.

Notes

The authors declare no competing financial interest.

ACKNOWLEDGMENTS

This work was supported by Grant-in-Aid for Challenging Exploratory Research (No. 2365116).

REFERENCES

(1) Auzel, F. *Chem. Rev.* **2004**, *104*, 139.
(2) Wang, F.; Liu, X. *Chem. Soc. Rev.* **2009**, *38*, 976.
(3) Wang, F.; Deng, R.; Wang, J.; Wang, Q.; Han, Y.; Zhu, H.; Chen, X.; Liu, X. *Nat. Mater.* **2011**, *10*, 968.

(4) Wang, F.; Han, Y.; Lim, C. S.; Lu, Y.; Wang, J.; Xu, J.; Chen, H.; Zhang, C.; Hong, M.; Liu, X. *Nature* **2010**, *463*, 1061.
(5) Haase, M.; Schäfer, H. *Angew. Chem., Int. Ed.* **2011**, *50*, 5808.
(6) Deng, R.; Xie, X.; Vendrell, M.; Chang, Y. T.; Liu, X. *J. Am. Chem. Soc.* **2011**, *133*, 20168.
(7) Peng, H. S.; Stolwijk, J. A.; Sun, L. N.; Wegener, J.; Wolfbeis, O. S. *Angew. Chem., Int. Ed.* **2010**, *49*, 4246.
(8) Achatz, D. E.; Meier, R. J.; Fischer, L. H.; Wolfbeis, O. S. *Angew. Chem., Int. Ed.* **2011**, *50*, 260.
(9) Liu, Y.; Wang, D.; Shi, J.; Peng, Q.; Li, Y. *Angew. Chem., Int. Ed.* **2013**, *52*, 4366.
(10) Dong, B.; Cao, B.; He, Y.; Liu, Z.; Li, Z.; Feng, Z. *Adv. Mater.* **2012**, *24*, 1987.
(11) Debasu, M. L.; Ananias, D.; Pastoriza-Santos, I.; Liz-Marzán, L. M.; Rocha, J.; Carlos, L. D. *Adv. Mater.* **2013**, *25*, 4868.
(12) Hao, J.; Zhang, Y.; Wei, X. *Angew. Chem., Int. Ed.* **2011**, *50*, 6876.
(13) Sun, Q. C.; Mundoor, H.; Ribot, J. C.; Singh, V.; Smalyukh, I. I.; Nagpal, P. *Nano Lett.* **2014**, *14*, 101.
(14) Rocha, J.; Carlos, L. D.; Paz, F. A. A.; Ananias, D. *Chem. Soc. Rev.* **2011**, *40*, 926.
(15) Li, J. R.; Kuppler, R. J.; Zhou, H. C. *Chem. Soc. Rev.* **2009**, *38*, 1477.
(16) Erdem, E.; Karapinar, N.; Donat, R. *J. Colloid Interface Sci.* **2004**, *280*, 309.
(17) Caro, J.; Noack, M.; Kölsch, P.; Schäfer, R. *Microporous Mesoporous Mater.* **2000**, *38*, 3.
(18) Schaak, R. E.; Mallouk, T. E. *Chem. Mater.* **2002**, *14*, 1455.
(19) Gopalakrishnan, J.; Bhat, V. *Inorg. Chem.* **1987**, *26*, 4299.
(20) Wang, F.; Wang, J.; Liu, X. *Angew. Chem., Int. Ed.* **2010**, *49*, 7456.

dx.doi.org/10.1021/ic501129y | *Inorg. Chem.* 2014, 53, 9151−9155